JOURNAL OF NEUROPHYSIOLOGY
Vol. 67, No. 5, May 1992. *Printed in U.S.A.*

Membrane Properties of Dentate Gyrus Granule Cells: Comparison of Sharp Microelectrode and Whole-Cell Recordings

KEVIN J. STALEY, THOMAS S. OTIS, AND ISTVAN MODY
Department of Neurology and Neurological Sciences M016, Stanford University School of Medicine, Stanford, California 94305

SUMMARY AND CONCLUSIONS

1. Whole-cell and sharp electrode recordings from adult rat dentate gyrus GCs were performed in the 400-μm-thick hippocampal slice preparation maintained at 34 ± 1°C. Intrinsic membrane properties of granule cells (GCs) were evaluated with the use of a switching current-clamp amplifier.

2. With the whole-cell technique, the average resting membrane potential (RMP) of GCs was −85 mV when a potassium gluconate electrode solution was used versus −74 mV measured with potassium acetate–filled sharp microelectrodes. The membrane voltage response to injected current was linear over two membrane potential ranges, >10 mV hyperpolarized from RMP and between 10 mV more negative than RMP and −62 mV. The average input resistances (R_N) calculated over these ranges were 107 and 228 MΩ in the whole-cell recordings versus 37 and 54 MΩ in the sharp electrode recordings. There was no correlation between RMP and R_N with either recording technique. The membrane time constant (τ_m) determined at the RMP was 26.9 ms for whole-cell recordings and 13.9 ms for sharp electrode recordings.

3. There was no evidence of time-dependent changes in RMP, R_N, and τ_m in whole-cell recordings, although the slow inward rectification seen at hyperpolarized potentials decreased over 30–60 min. Addition of calcium buffers to the whole-cell recording solution did not result in a significant change in the average RMP, the average R_N, or the average τ_m.

4. Action potential threshold was comparable in whole-cell (−49 mV) and sharp electrode (−52 mV) recordings, but action potential amplitude was larger in whole-cell (126 mV) than in sharp electrode (106 mV) recordings. Spike frequency adaptation was present in the whole-cell recordings and could be abolished by addition of calcium buffers to the electrode solution.

5. We estimated ρ, the ratio of dendritic to somatic conductance, to be 5.1 for the whole-cell records and 2.1 for sharp electrode recordings. The electrotonic length of the equivalent cylinder representing the cell processes was estimated to be 0.49 from the whole-cell data and 0.79 from the sharp electrode recordings. This implies that at rest there is only a 10% decrement in steady-state membrane voltage along the length of the dendrite due to shunting across the membrane resistance; small synaptic events occurring in the distal dendritic tree will therefore have a more substantial influence on the soma than previous analyses suggested.

6. The difference in R_N in sharp and whole-cell records is due to a conductance that is distributed over the cell soma and processes, has little time dependence, reverses near the RMP, and has a magnitude that is not correlated with the RMP. These results support the hypothesis that the additional conductance results from a combination of a nonspecific, electrode-associated leak conductance and a potassium conductance that is modulated by ionic flux through the leak conductance.

INTRODUCTION

Current understanding of the electrotonic structure of dentate gyrus GCs is based on studies that applied Rall's model of the neuron, in which the soma is represented by a lumped RC circuit and the cell processes are represented by an equivalent sealed-end cable (cf. Rall 1969, 1977), to experimental data obtained from sharp electrode recordings in the hippocampal slice preparation (Brown et al. 1981; Durand et al. 1983). These studies, together with a number of other investigations of the electrophysiology (Biscoe and Duchen 1980; Brown et al. 1981a; Crunelli et al. 1983; Fournier and Crepel 1984; Fricke and Prince 1984; Lambert and Jones 1990; McNaughton et al. 1981; Mody et al. 1988) and anatomy (Desmond and Levy 1984) of the dentate GCs, indicated that the GC had an input resistance (R_N) of ~45 MΩ (range 30–87) and a dendritic electrotonic structure that resulted in a 33–40% DC voltage drop along the length of the dendrite. These results implied that a substantial fraction of the voltage signal generated at synapses in the distal dendrites was shunted across the cell membrane before reaching the soma. In addition, because of the magnitude of the voltage drop along the dendrite, voltage-clamp studies of GC synaptic physiology appeared to be impractical.

The recent application of the patch electrode whole-cell recording technique (Hamill et al. 1981) to the brain slice preparation (Blanton et al. 1989; Edwards et al. 1989; Mody and Otis 1989) is providing a number of significant new insights into problems in synaptic physiology (Hestrin et al. 1990; Malinow and Tsien 1990). Although it has become clear that the R_N, space clamp, and signal-to-noise ratio are increased in the whole-cell recordings, the nature and extent of these changes have not been examined in detail.

We investigated electrotonic structure of the dentate GC with the use of data from both whole-cell and sharp electrode recordings, utilizing experimental protocols and analyses similar to those that had been used in the earlier sharp electrode studies. One complication of the whole-cell recording technique is the alteration of intracellular homeostasis caused by diffusion of critical intracellular constituents into the electrode solution (Horn and Marty 1988; Pusch and Neher 1988). Such alterations could affect the accuracy of our analysis, particularly if changes in intracellular free calcium levels activated a calcium-dependent potassium conductance. Therefore we also investigated the membrane properties of a group of GCs in which intracel-

lular calcium had been buffered to 2×10^{-8} M. In addition, the stability of the membrane properties over time was determined in cells without exogenous calcium buffers or sources of high-energy phosphates.

METHODS

Slice preparation

Adult (60–120 days old, 250–350 g) male Wistar rats were decapitated under pentobarbital sodium anesthesia (75 mg/kg ip), and their brains were removed. Brains were cooled in 4°C artificial cerebrospinal fluid (ACSF), composed of (in mM): 126 NaCl, 2.5 KCl, 26 $NaHCO_3$, 2 $CaCl_2$, 2 $MgCl_2$, 1.25 NaH_2PO_4, and 10 glucose. Coronal whole-brain slices (400 μm thick) were prepared with the use of a vibratome tissue sectioner (Lancer Series 1000). The brain slices were then sagitally bisected into two hemispheric components and incubated submerged in a storage chamber at 32°C. Warmed and humidified 95% O_2-5% CO_2 flowed over the top of the slices maintained at 34 ± 1 (SE) °C. A ×50 dissecting microscope was used to view the dentate GC layer during electrode placement.

Electrodes

Patch electrodes were pulled from borosilicate glass capillary tubing (1.5 mm OD; KG-33, Garner Glass, Claremont, CA) with the use of a Narishige PP-83 two-stage electrode puller. Tip dimensions were 0.5–1.0 μm ID and 3–4 μm OD. Electrode tip diameter was checked with an air interface ×400 microscope. The tips were not fire polished and coatings were not used.

The intracellular patch electrode solution was composed of (in mM): 135 potassium gluconate, 5 KCl, 2 $MgCl_2$, and 10 *N*-2-hydroxyethylpiperazine-*N'*-2-ethanesulfonic acid (HEPES), the solution was buffered to pH 7.20 with KOH. In some experiments, chloride was used in place of gluconate. The calculated Nernst equilibrium potential at the GC membrane for potassium (E_K) at 34°C, assuming rapid equilibration of the electrode solution and cytoplasmic ion concentrations (Pusch and Neher 1988) and an 0.75 activity coefficient for the internal concentration of potassium gluconate (Vanysek 1988), was −98 mV. In other experiments, the tetrapotassium salt of 1,2-bis(2-aminophenoxy) ethane-*N,N,N',N'*-tetraacetic acid (BAPTA) and $CaCl_2$ were substituted for potassium gluconate. The ratio of BAPTA to $CaCl_2$ was 11:1 mM in most experiments; this buffered the internal free calcium to a calculated value of 20 nM at 34°C (Harrison and Bers 1987; Pethig et al. 1989). In some cells, the BAPTA-to-$CaCl_2$ ratio was increased to 20–0.5 mM to buffer the free calcium to 5 nM; the results from these cells are noted separately in the text. The potassium concentration in buffered and unbuffered solutions was 135 mM; final osmolarity for all solutions was 260–280 mOsm. To estimate the free calcium contaminating the unbuffered electrode solution, the free calcium concentration was measured in a sample of unbuffered electrode solution with the use of fura-2 (Grynkiewicz et al. 1985) and found to be 60–80 nM.

Compressed Ag/AgCl pellet electrodes (E. F. Wright) were in contact with the electrode fill solution and ACSF. No electrode polarization was detected at the current amplitudes used in this study. The junction potential at the electrode tip due to the differing mobilities of the ions in the electrode and bath solutions was measured as described by Hagiwara and Ohmori (1982). These values (10 mV for potassium gluconate and potassium gluconate/BAPTA; 3 mV for KCl) were subtracted from the recorded membrane voltage of the whole-cell recordings.

Sharp microelectrodes were pulled from 1-mm OD glass. The electrodes were filled with 3 M potassium acetate. Sharp electrode access resistances were in the range of 80–110 MΩ.

Recordings

Determination of the electrotonic parameters of hippocampal neurons involves the analysis of voltage transients that decay multiexponentially; some of the time constants are <1 ms (Brown et al. 1981a; Johnston 1981; Rall 1969). The critical requirements for accurate measurement of the short time constants are an adequate recording bandwidth and minimization of filtering due to the electrode resistance in series with the membrane capacitance (Finkel and Redman 1985; Wilson and Park 1989). These short time constants will be underestimated if the recording bandwidth is inadequate and overestimated if resistive electrode voltage errors are present. To minimize voltage errors due to electrode resistance, we used a switching amplifier (Axoclamp 2A, Axon Instruments) to inject current and measure the membrane voltage (V_M). A compensation circuit was used to cancel electrode capacitance, but the thick walls of the patch electrode kept this capacitance minimal when the fluid layer over the slice was ≤300 μm. The switching frequency was set at 5–7 kHz, depending on the settling time of the electrode.

The switching single-microelectrode recording technique requires that the time constant of the electrode be much shorter than the shortest measured neuronal time constant (Finkel and Redman 1985). Figure 1 shows typical instantaneous electrode voltage responses during current injection. The voltage response of the electrode (*V*mon) decayed monoexponentially when the electrode was in the ACSF with a time constant of 30–50 μs; capacitance compensation had minimal effect on this time constant at submersion depths <300 μm. After formation of the whole-cell recording configuration, the DC resistance usually increased to 10–20 MΩ and the electrode time constant increased to 100–200 μs. Presumably, the increased time constant was due to partial obstruction of the tip with membrane constituents. The electrode time

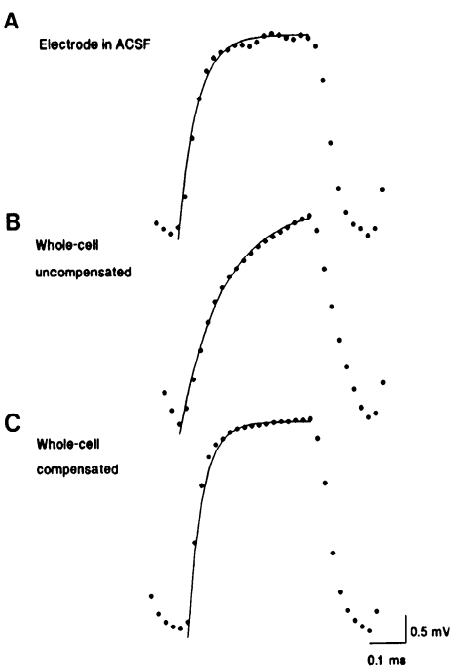

FIG. 1. Patch electrode voltage settling in discontinuous current clamp. Figures are instantaneous headstage voltages during injection of −200 pA; switching frequency decreased to 2 kHz to improve digitization for illustration. *A*: electrode voltage with tip in ACSF. Monoexponential electrode response (τ = 0.05 ms) without capacitance compensation. *B*: after formation of whole-cell recording configuration, τ = 0.11 ms without capacitance compensation. *C*: with capacitance compensation, τ decreases to 0.04 ms. Voltage calibration refers to *C*; *A* multiplied by 6.0, and *B* multiplied by 1.4.

constants were shortened with capacitance compensation to 25–40 μs. At switching frequencies of 5–7 kHz with 30% of each cycle used for passing current, the electrode voltage decayed for four electrode time constants. Electrodes that did not settle adequately within 200 μs (i.e., could not be switched at ≥5 kHz) during intracellular recordings were discarded. The adequacy of the electrode settling was monitored continuously, although adjustments in capacitance compensation were rarely necessary, because electrode deterioration was a rapid, all-or-none phenomena.

Sharp electrode recordings were made after stabilization of the membrane voltage. The same recording techniques were used for the sharp electrodes, although capacitance compensation was frequently not as optimal as for the patch electrodes. Switching frequency for the sharp electrodes varied between 4 and 6 kHz.

The outputs of the amplifier were filtered at 0–10 kHz (−3 dB), digitized at 44 kHz with a 14-bit pulse code modulated digitizer (Neuro Data DR-484), and recorded on videotape for off-line analysis.

Seal formation

The superior (dorsal) blade of the dentate gyrus was identified with the use of the ×50 dissecting microscope. The electrode was advanced into the fluid over the GC layer, and the electrode potential was set to zero. The amplifier was set to continuous ("bridge") mode and current pulses (−120 pA × 20 ms, repeated every 100 ms) were injected. The electrode resistance in the extracellular fluid was 3–6 MΩ. The electrode resistance was monitored by observing the change in electrode potential during the current pulse.

The electrode was advanced into the GC layer in 2- to 5-μm increments. When the electrode was adjacent to a GC, the electrode resistance increased by 5 MΩ (Fig. 2*A*). At this point, suction was applied to the electrode via a 10-ml syringe attached by flexible PVC tubing to the electrode holder. Very small (<0.5 ml) displacements of the syringe resulted in an increase in the electrode (seal) resistance of several hundred megohms and the appearance of a slow charging curve. The seal resistance then increased over the next 10–40 s to a stable value of >1 GΩ. (Because the time constant of the seal was much greater than 20 ms, the 1 GΩ value represents a substantial underestimate of the actual seal resistance). At this point, the cell membrane was considered to be well sealed to the electrode tip. When the apparent seal resistance was >1 GΩ, steady suction applied orally via the PVC tubing to the electrode resulted in a drop in resistance to 1–300 MΩ and the appearance of a potential in the absence of a current pulse. At this point, the cell membrane within the lumen of the electrode tip was considered to be broken, and the potential was considered to represent the resting membrane potential (RMP). The RMP was corrected at the conclusion of the experiment if, after withdrawal of the electrode, a potential was present with the electrode in the extracellular space.

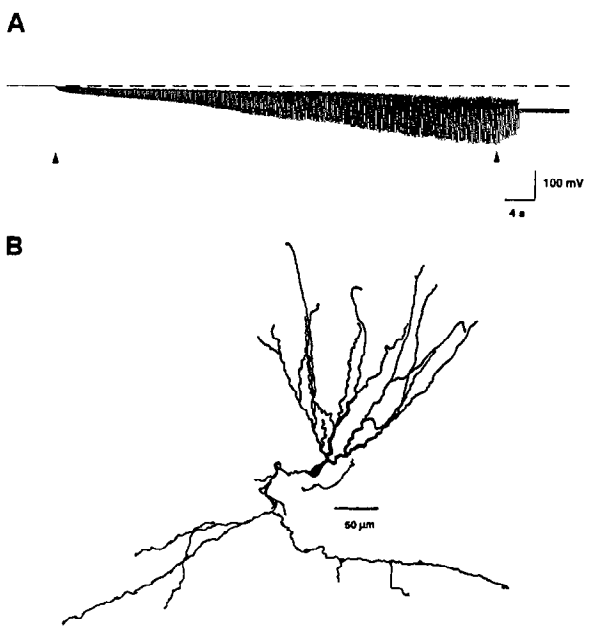

FIG. 2. *A*: strip chart recording of electrode voltage response to −120-pA current steps during formation of whole-cell seal. 1st arrow indicates the 1st application of suction to form cell-attached seal. Voltage deflections just before first suction cannot be seen at this gain, but are ~0.5 mV. After the 1st suction, seal resistance increases rapidly; when voltage change 20 ms after current step is >120 mV, gentle suction is applied (▲) to rupture the cell membrane within the lumen of the electrode. This membrane rupture is signified by the sudden change in time constant and registration of membrane potential. Voltage deflections after membrane rupture indicate the stability of R_N during the initial equilibration of electrode and cytoplasmic solutions. Dashed line indicates the 0 mV potential. *B*: camera lucida drawing of a biocytin-filled GC.

Sharp and whole-cell recordings from GCs were included in the study when neurons had RMPs more negative than −65 mV, R_N >25 MΩ, and overshooting action potentials. Cells with a large, stable RMP (more negative than −80 mV) but very short membrane time constant, low R_N, and no action potentials were found in 10% of recordings. These properties did not change over periods of ≤30 min. These cells were presumed to be glial cells and are not considered further in this study.

Protocols

After the stabilization of the RMP and adjustment of the switching frequency and capacitance compensation, the current-voltage relationship of the granule cells (GCs) were determined with the use of 300-ms current steps every 2 s. The current step amplitude began at −300 pA and was increased every four steps in either 100- or 50-pA increments to a maximum of +200 pA. 200 ms after the start of each step, an additional −100 pA-50 ms square current step was added (Fig. 7). For the purposes of the current-voltage relationship and determination of the R_N, V_M was measured 180 ms after the start of the initial current step. The time between patch rupture and *I-V* determination was typically 2 min and always <5 min. Membrane time constants were determined from the first 50 ms of the voltage response to a +50-pA current step. In a second protocol, 2 ms-+200 pA current steps were used instead of the 50 ms-−100 pA current steps to improve the resolution of the shorter membrane time constants; the first 35 ms of voltage decay after this step were used to determine the membrane time constant (Durand et al. 1983).

Data analysis

Taped data were redigitized for analysis on an Intel 80286/80287-based computer with the use of the Strathclyde Electrophysiology software. Redigitization sampling rate was 6 kHz, and data were filtered with a bandpass of DC to 3 kHz (−3 dB). R_N was computed as the slope of the current-voltage plot (least-squares fitted line) over the linear range near RMP. Because V_M for a particular current step varied from cell to cell depending on R_N, data points for membrane potential were binned in 5- or 10-mV increments for plotting and for standard error determinations. Spike threshold was determined from voltage responses to depolarizing current steps. The potential at which the slope of the membrane potential charging curve first increased was determined by eye, and the potential at that point was taken to be the spike threshold. Spike height was calculated as the difference between the RMP and the most positive segment of the action potential. Membrane time constants were determined by one- or two-

exponential curve fitting with the use of a modification of the Levenberg-Marquardt least-squares algorithm (Brown and Dennis 1972). Estimates of the statistical significance of the differences in the means were calculated with the use of Student's two-tailed t test (Snedecor and Cochran 1975).

Rall has derived the expressions describing the behavior of a neuron model consisting of a lumped RC circuit representing the cell soma in series with a distributed RC circuit representing the cell processes (Rall 1977). The voltage response to a long current step contains an exponential term because of the charging of the membrane capacitance. In addition, there are exponential terms with shorter time constants that are due to the redistribution of charge from the site of current injection to more distal sites

$$V(t) = \sum_{i=0} C_i \times e^{(-t/\tau i)}$$

Where $V(t)$ is the voltage at time t, C_i are the appropriate constants for $t = 0$, τ_0 is the membrane time constant (τ_m), and $\tau_1 \cdots \tau_n$ are the time constants for the redistribution terms. The initial milliseconds of the voltage response to a current step were poorly fit when only one exponential term was used but fit a biexponential decay well. Although there are theoretically many more equalizing terms, we could not resolve them given the bandwidth of our recordings.

In comparing the sharp versus whole-cell R_N, it was important to estimate ρ, the ratio of dendritic to somatic transmembrane conductance (Rall 1969, 1977). Several methods of calculating ρ are available; we used the method of Brown (Brown et al. 1981b)

$$\rho = [(\tau_0/V) \times \sum_{i=0} (C_i/\tau_i)]^{-1}$$

Because this method assumes an infinite number of redistribution terms, when in fact we could resolve only two, ρ will be underestimated. The real ratios of dendritic-to-somatic conductance are thus somewhat higher than indicated in the table; Brown et al. estimated the error to be 37%. However, because estimates of ρ derived from both the sharp and whole-cell data are subject to the same error, comparisons of values for ρ derived from the two recording techniques are still accurate. The more precise methods of calculating ρ (Johnston 1981) could not be applied to our data because, as pointed out by others (Brown et al. 1981a), the equations involved can only be evaluated when the cell charging curves are more nearly monoexponential.

The electrotonic length (L) of the sealed-end equivalent cylinder that describes the GC processes was calculated with the use of an implementation (Brown et al. 1981a,b) of Rall's model (Rall 1969, 1977) and the previously calculated value of ρ

$$L_{\text{estimated}} = \pi \times [\rho/(\rho + 1)]^{1/2}/\alpha$$

$$\rho = -\alpha \times \cot(\alpha L) \times \tanh(L)$$

where

$$\alpha = [(\tau_0/\tau_1) - 1]^{1/2}$$

L is the length of the equivalent sealed-end cylinder, expressed as a multiple of the length constant, λ; λ is the ratio of the membrane to intracellular resistivity (in the infinite cylinder model, λ is the distance at which the membrane voltage falls to e^{-1} of the voltage at the origin). L is derived from the best fit to the transcendental equation used to express ρ. $L_{\text{estimated}}$ is used as a starting point, because the expression of ρ yields an infinite number of solutions. We made certain that the value of $L_{\text{estimated}}$ was close to one of the roots by plotting ρ as a function of the fitted L.

We also estimated the electrotonic length (L_C) of a simpler sealed-end cylinder model that described the GCs. In this model, the cylinder represents the whole neuron, and the somatic conductances are combined with the conductances of the cell processes. We used the expression derived by Rall

$$L_C = \pi \times [(\tau_m/\tau_1) - 1]^{-1/2}$$

Finally, from the definition of ρ and the measured R_N, the R_N of the equivalent cylinder representing the cell processes can be determined (Rall 1977)

$$R_D = R_N \times (1 + 1/\rho)$$

Histology

To ascertain that the cells that we recorded were in fact GCs, patch electrodes were in some instances filled with an electrode solution containing 0.1% biocytin. At the end of the recording, the slice was removed from the recording chamber and fixed overnight in 4% paraformaldehyde. Histochemical processing with the use of an avidin/horseradish peroxidase label was as described by Horikawa and Armstrong (1988).

RESULTS

Anatomy

We attempted to fill 20 cells with 0.1% biocytin. Our success rate was limited by somatic damage that occurred when the electrode was withdrawn at the end of the recording. Thus the majority of stain failures consisted of cells with well-filled processes but disrupted soma. Some nonspecific staining of the surrounding tissue was seen even in the cells that were not disrupted on removal of the electrode. This was probably due to diffusion of electrode solution before seal formation and during withdrawal of the electrode at the end of the recording. All six of the cells that were successfully stained (Fig. 2*B*) had morphologies characteristic of GCs (Seress and Pokorny 1981). Although we did not identify the majority of the study cells morphologically, it is unlikely that the neurons were other than GCs on the basis of our successful stains and the ratio of GCs to interneurons identified in other studies (Durand et al. 1983). Further, none of the study cells demonstrated electrophysiological characteristics of interneurons, such as short, nonadapting interspike interval (Kawaguchi and Hama 1987).

Resting membrane potential

The characteristics of GCs recorded with whole-cell and sharp electrodes are tabulated in the table. The average RMP of the GCs was −74 mV in the sharp electrode recordings. This is well within the range (−65 to −85 mV) reported by other investigators (Biscoe and Duchen 1980; Brown et al. 1981; Crunelli 1983; Durand et al. 1983; Fournier and Crepel 1984; Lambert and Jones 1990; McNaughton et al. 1981; Mody et al. 1988).

The average RMP of the GCs was −84 mV in the whole-cell recordings. This is more negative than the −67 mV RMP reported for room temperature whole-cell recordings of GCs utilizing 140 mM KCl, ethylene glycol-bis(β-aminoethyl ether)-*N,N,N′,N′*,-tetraacetic acid (EGTA)-containing electrode solutions in 100- to 200-μm-thick hippocampal slice preparations from 3-wk-old rats (Edwards et al. 1989). As shown in the table, calcium buffering had no effect on the RMP in our study, indicating that the dif-

ference between the RMP reported by Edwards et al. (1989) and our study was not due to differential activation of a calcium-dependent potassium conductance. With the use of an electrode chloride concentration equivalent to that of Edwards et al. (1989), we measured an average RMP of −74 mV. The RMP measured in the present study may be more negative than the RMP reported by Edwards et al. (1989) because of minor differences in junction potential correction in addition to the depolarizing effect of lower recording temperature (Hakozaki et al. 1989; Shen and Schwartzkroin 1988) and the smaller RMP seen in younger animals (Kriegstein et al. 1987). The depolarizing effect of the high intracellular chloride concentration in our study and that of Edwards et al. (1989) is consistent with the predictions of the Goldman voltage equation due to resting membrane chloride permeability. Some of this permeability is due to chloride channels that are activated by endogenous γ-aminobutyric acid (GABA) acting through $GABA_A$ receptors (Ben-Ari et al. 1989; Otis et al. 1991; Thompson et al. 1988; Thompson and Gähwiler 1990).

The significance of the difference in RMP measured with the sharp and whole-cell electrodes is affected by three factors. First, the accuracy of the sharp electrode measurements may be affected by small, uncorrected junction potentials (Cole and Moore 1959) and tip potentials (Gagne and Plamondon 1982); the accuracy of the whole-cell junction potential correction (Hagiwara and Ohmori 1982) is affected by similar sharp electrode errors. Second, if ions in the cytoplasm rapidly equilibrate with ions in the patch electrode (Pusch and Neher 1988), then the reversal potential of the ionic conductances that contribute to the RMP are completely and somewhat artificially determined in the whole-cell recordings by the relative ionic concentrations in the electrode solution and the ACSF. Similarly, the transmembrane ion gradients are altered by the sharp electrode solution, although in a less quantifiable way; comparisons of the RMPs measured with the two techniques are not easily corrected for these effects. Third, if the ions in the patch electrode solution and the cytoplasm do not completely equilibrate, then the RMP in the whole-cell recordings will be too negative because of an overcorrection for the junction potential.

Action potential characteristics

Spike threshold was similar for the whole-cell and sharp electrode recordings (Table 1). The magnitude of the current injection and corresponding rate of rise of the membrane voltage did not change the spike threshold by >1 mV over a current range of 100–400 pA in the sharp and whole-cell recordings (Fig. 4). In four of the whole-cell recordings, spike threshold was evaluated over a 30- to 60-min recording interval; the threshold for these cells was −47 ± 0.2 initially and −48 ± 2.1 later. Judging from previously published figures, our values for spike threshold appear to be similar to what other investigators have found, although these data have not been reported systematically in previous studies of GC electrophysiology (Biscoe and Duchen 1980; Brown et al. 1981; Crunelli 1983; Durand et al. 1983; Fournier and Crepel 1984; Lambert and Jones 1990; McNaughton et al. 1981; Mody et al. 1988).

TABLE 1. *Membrane properties of granule cells in sharp electrode vs. whole-cell recordings*

	Sharp Electrode	Patch Electrode	Patch Electrode + BAPTA
n	11	31	10
RMP, mV	−74 ± 2.1	−84 ± 1.0	−84 ± 0.9
Spike threshold, mV	−52 ± 1.5	−49 ± 0.8	−49 ± 0.3
Spike height, mV	106 ± 3.2	126 ± 3.8	127 ± 2.2
R_N, MΩ	54 ± 3.0	228 ± 14.2	186 ± 23.0
τ_1, ms	1.2 ± 0.2	0.81 ± 0.05	0.77 ± 0.08
τ_0, ms	13.9 ± 1.6	26.9 ± 1.2	23.6 ± 1.7
L, cell	0.95 ± 0.06	0.56 ± 0.02	0.60 ± 0.03
ρ	2.1 ± 0.37	5.1± 0.35	5.3 ± 0.49
L, dendrite	0.72 ± 0.08	0.47 ± 0.02	0.51 ± 0.02
R_D, MΩ (dendritic input *R*)	61 ± 5	255 ± 16	200 ± 34

All of the listed mean values (±SE) of the plain patch electrode recordings were significantly different from the mean values of the sharp electrode recordings ($P < 0.001$, two-tailed *t* test) except for spike threshold (not significant), and τ_1 ($P < 0.005$). None of the BAPTA mean values were significantly different from the mean values of the plain patch recordings. BAPTA, 1,2-bis(2-aminophenoxy)ethane-*N*,*N*,*N*′,*N*′-tetraacetic acid; RMP, resting membrane potential; R_N, input resistance; τ_1, τ_0, shorter equalizing and longer membrane time constants, respectively; L, length of the equivalent sealed-end cylinder; ρ, ratio of dendritic to somatic conductance; R_D, input resistance of the dendritic equivalent cylinder.

The spike amplitude recorded with the sharp electrodes was higher than that reported in previous sharp electrode studies (Fournier and Crepel 1984; Godfraind 1985; Mody et al. 1988), and the spike amplitude measured with the whole-cell electrodes was larger than the amplitude measured with sharp electrodes (Table 1). Because action potentials approximate delta functions, the measured spike height is strongly dependent on recording bandwidth. The variation in spike amplitude among the studies may then be due to the differences in high frequency response of the recording techniques, although we have not evaluated the contribution of other factors such as the differences in the permeability and reversal potential of sodium.

Adaptation of spike frequency is illustrated for whole-cell recordings in Fig. 3. Although spike frequency adaptation was not studied quantitatively, qualitative evaluation provided a means of assessing adequacy of calcium buffering in the whole-cell recordings. Spike frequency adaptation could be demonstrated in cells recorded without added exogenous calcium buffers (Fig. 3). This situation resembles findings in acutely dissociated neurons, where recordings without any exogenous intracellular calcium buffers accurately reflect the intracellular endogenous calcium-buffering capacity of neurons established with the perforated patch method (Köhr and Mody 1991), which does not interfere with intracellular calcium homeostasis (Horn and Marty 1988). Thus, in the recordings made without exogenous calcium buffers, intracellular calcium homeostasis was not altered to the point of affecting calcium-dependent potassium conductances, which have been shown to underlie adaptation of spike frequency in hippocampal neurons (Lancaster and Adams 1986; Madison and Nicoll 1984). In the cells recorded with 11 mM BAPTA-1 mM $CaCl_2$ (Fig. 3), spike frequency adaptation was blocked within 1–2 min after formation of the whole-cell recording configuration

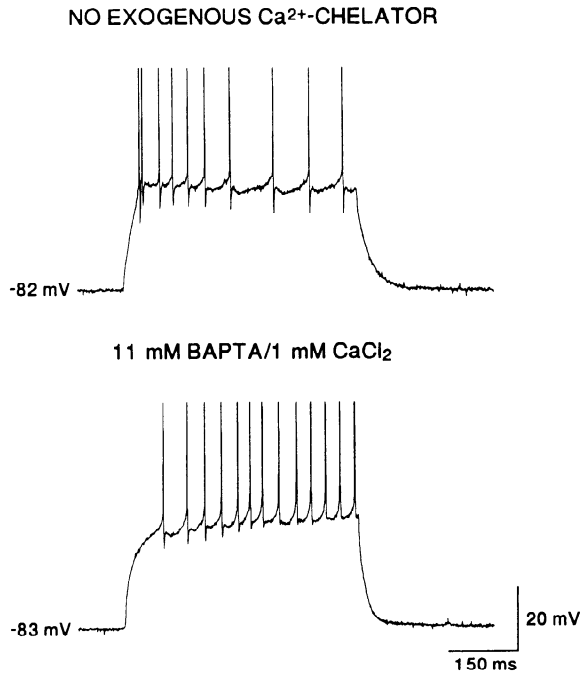

FIG. 3. Adaptation of action potential frequency in whole-cell recordings during 300-ms/200-pA current steps in 2 different GCs. *Top*, recorded 8 min after intraluminal membrane rupture, from a cell without exogenous calcium buffers in the recording electrode. *Bottom*, from a cell recorded with the calcium chelator BAPTA in the electrode solution (11 mM BAPTA-1 mM $CaCl_2$), 10 min after membrane rupture. Note the lack of spike frequency adaptation and the gradual abolishment of post-spike afterhyperpolarizations.

(the earliest time at which depolarizing current steps were applied), as has been demonstrated with sharp microelectrode BAPTA studies (Lancaster and Nicoll 1987). The presence of fast calcium-dependent afterhyperpolarizations during the early spikes in the train are most likely due to the kinetic ineffectiveness of the BAPTA-dependent calcium binding, which is usually not sufficient to prevent the occurrence of very fast calcium-dependent conductances even at BAPTA concentrations as high as 30 mM (Llano et al. 1991). We were not able to abolish the initial spike afterhyperpolarizations even in four cells recorded with the use of a 20-mM BAPTA-0.5-mM $CaCl_2$ (calculated free calcium level of 5 nM) electrode solution.

Current-voltage relationships

GC membrane potential responses to long (200-ms) current steps recorded with sharp electrode and whole-cell techniques are shown in Fig. 4. Figure 5 summarizes the membrane voltage responses to current steps in 31 neurons studied with the whole-cell technique and 11 cells recorded with sharp electrodes. There are two regions in which the current-voltage relationship is linear.

In whole-cell recordings, the *I-V* relationship was linear between −95 and −62 mV, and the R_N was 228 MΩ. Above +100 pA, the *I-V* data could not be reliably averaged, because action potentials and afterhyperpolarizations contaminated the voltage response in cells with higher R_Ns (Figs. 3 and 4). There was no significant correlation between R_N

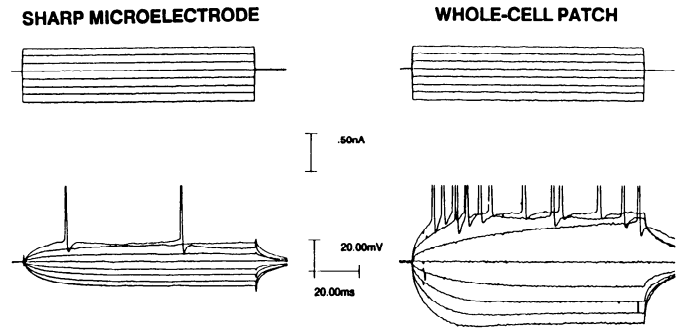

FIG. 4. Comparison of membrane voltage responses to current steps in GCs recorded with sharp electrode vs. whole-cell patch electrode. Sharp electrode filled with 3 M potassium acetate. The differences in R_N and τ_m can be appreciated by visual inspection of the records. Spike threshold is similar for the 2 recording methods.

and RMP ($r = 0.09$). At potentials more negative than −95 mV, the voltage response was also linear with a slope of 107 MΩ. In this region, voltage sags typical of a slow inward rectifier current (I_Q, Adams and Halliwell 1982; Hotston et al. 1979), can be seen (Figs. 4, 5, and 7*B*). The increase in conductance in this voltage region was estimated to be 5.0 nS in the whole-cell recordings (see APPENDIX). Our experiments did not address the reversal potential or permeability of the channels underlying the additional conductance; hyperpolarization-activated conductances that are permeable to both sodium and potassium have been described in other preparations (McCormick and Pape 1990).

In the sharp electrode recordings, the *I-V* relationship was linear between −85 and −62 mV, with an R_N of 54 MΩ. The same population-averaging considerations encountered in the whole-cell recordings made evaluation of the *I-V* relationship at more depolarized potentials inaccurate. The average R_N is well within the range of values obtained by other investigators with the use of similar techniques (Biscoe and Duchen 1980; Brown et al. 1981; Crunelli et al. 1983; Durand et al. 1983; Fournier and Crepel 1984; Lambert and Jones 1990; McNaughton et al. 1981; Mody et al. 1988). There was no significant correlation between R_N and RMP ($r = 0.18$). The response was also linear with a

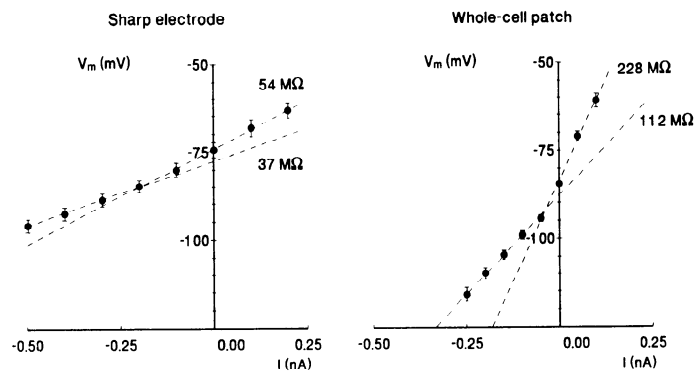

FIG. 5. Membrane voltage vs. injected current for 31 GCs recorded in whole-cell method and 10 GCs recorded with sharp electrodes; points are means + SE. Voltage was determined 180 ms after start of current pulse. Error bars indicate SE. Lines are fitted by least-squares method. Regions of linearity determined by eye.

slope of 37 MΩ at potentials between −85 and −100 mV (Fig. 5); voltage sags due to I_Q activation were seen in this range. The increase in conductance in this voltage region was estimated to be 8.5 nS (see APPENDIX).

The voltage at which the slow inward rectifier clearly decreased the slope of the *I-V* relationship was 10 mV hyperpolarized from RMP in both the sharp and whole-cell recordings. In voltage-clamp studies in other preparations, the slow inward rectifier conductance begins to activate at potentials more negative than −60 mV (McCormick and Pape 1990; Segal and Barker 1984) and inactivates slowly. The change in the slope of the *I-V* curve at −10 mV hyperpolarized to RMP may indicate that I_Q begins to activate at more negative membrane potentials in dentate gyrus GCs. However, our current-clamp data are not adequate to address the voltage-dependent activation of I_Q in more detail.

The high R_N of the GCs cannot be attributed to the suppression of a conductance secondary to diffusion of intracellular constituents out of the cell into the patch electrode. According to Pusch and Neher (1988), diffusion of substances in and out of cells is directly related to their molecular weight. Thus nucleotides that have molecular masses of ~1,000 Da should diffuse out of the neuron with time constants <2 min. We had an excellent estimate of the neuronal R_N immediately on breakthrough on the basis of membrane voltage deflection caused by the 100–120 pA/20 ms current pulses used to monitor the seal resistance (e.g., Fig. 2*A*). This initial R_N did not change in a time-dependent fashion, as would be expected if the conductances responsible for R_N were affected by a rapid diffusion of nucleotides (Pusch and Neher 1988). Yet it is likely that nucleotides diffuse into the patch pipette, because guanidinetriphosphate (GTP)-dependent $GABA_B$ responses are difficult to observe unless GTP is included in the recording solution (T. S. Otis and I. Mody, unpublished data). The stability of the *I-V* relationship in whole-cell recordings is shown for longer periods of time in Fig. 6. The primary effect noted over prolonged recording periods of 30–60 min was a small hyperpolarizing shift in the resting potential and a diminution of I_Q. The small rundown of I_Q over long recording periods is interesting because it suggests that this conductance may be modulated by some metabolic changes or by large molecular weight factors (Pusch and Neher 1988) whose concentration may have decreased over 30–60 min because of slow diffusion into the electrode solution, whereas the conductances responsible for the R_N were unchanged.

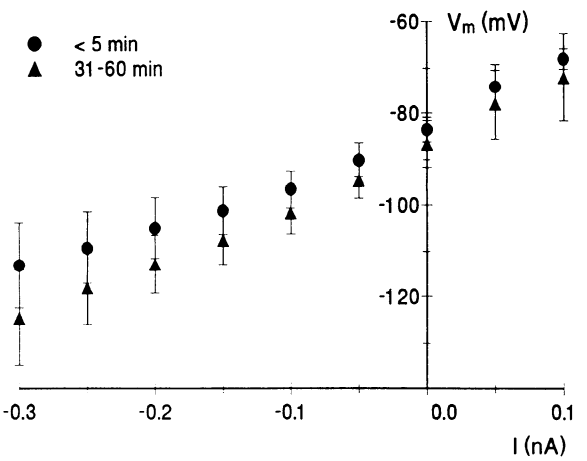

FIG. 6. Membrane voltage vs. injected current: stability over time. Data from 4 GCs; 1st current-voltage data were recorded within 5 min of start of recording, and second current voltage data obtained after 30–60 min; average interval between data sets was 42 min. The effect of I_Q is not as evident in the later records.

The average R_N of cells loaded with an exogenous calcium chelator (Table 1) was slightly lower than the average R_N of GCs in which calcium buffers were not used, but this difference was not statistically significant. Thus, although intracellular BAPTA prevented adaptation of spike frequency, it did not decrease any steady-state conductances active near RMP. Slow calcium-dependent conductances such as I_{AHP} (Lancaster and Adams 1986) are thought to be activated by calcium concentrations in the nM range (Brown 1990). Because the R_N of the buffered cells was no larger than the R_N of the unbuffered cells, the calcium homeostasis in the unbuffered cells was clearly intact enough to prevent substantial steady-state activation of such calcium-dependent conductances. The integrity of the endogenous calcium homeostatic mechanisms has also been demonstrated in unbuffered whole cell recordings of calcium currents in acutely dissociated GCs (Köhr and Mody 1991).

Although the small difference in R_N between the buffered and unbuffered cells was not statistically significant, we were concerned that the difference might reflect an unexpectedly lower level of free calcium in the unbuffered cells relative to the BAPTA cells. Therefore four cells were recorded with the use of 20 mM BAPTA-0.5 mM $CaCl_2$, so that the calculated free calcium level was 5 nM. In these cells, the average R_N was 193 MΩ, indicating that the small difference in R_N between the buffered and unbuffered cells was more likely related to sample size rather than a higher free calcium level in the buffered cells.

The average R_N of the whole-cell recordings was lower than the average R_N of the cells recorded with the thin slice technique (Edwards et al. 1989). As demonstrated by Storm (1990), this difference is largely explained by differences in the age of the animals used (3 wk vs. 3 mo). Differences in temperature (24 vs. 34°C) (Hakozaki et al. 1989; Shen and Schwartzkroin 1988) and the number of cell processes left intact in the 100- to 200-μm versus the 400-μm-thick slice preparations may also contribute to the lower R_N measured in our cells.

The difference in average R_N in cells recorded with the sharp and whole-cell techniques is large and suggests that if the whole-cell R_N is the "true" R_N, an additional conductance equal to three times the resting conductance of the cell is present in the sharp electrode recordings (see APPENDIX). The nature of this additional conductance is discussed below.

Membrane time constants

The time constants of the charging curves for the sharp and whole-cell recordings are listed in Table 1. The sharp electrode time constants are similar to those obtained by

other investigators with the use of similar methods (Brown et al. 1981; Crunelli et al. 1983; Durand et al. 1983). The time constants obtained from whole-cell recordings are notable for a longer membrane time constant (τ_0) and a shorter equalizing time constant (τ_1). A longer τ_0 is expected given the increased R_N; the relative differences in R_N and τ_0 between the sharp and whole-cell recordings are considered in greater detail below. The shorter τ_1 may have been due to a better high-frequency response in the whole-cell recordings. To ascertain that the shorter τ_1 was not due to inaccurate exponential fitting, the voltage decay after a short current step was also evaluated. As shown in Fig. 7*A*, the voltage decay after a short current step is determined primarily by τ_1 when the step duration is much shorter than τ_0 (Durand et al. 1983). With the use of this protocol, we confirmed the average τ_1 value of 0.8 ms in 20 of the 31 GCs recorded with the whole-cell technique. The average τ_0 when the short pulse protocol was used was 24.8 ms.

We also observed a voltage dependence of τ_0 (Fig. 7). Although we quantified this only for the whole-cell recordings, it is also apparent in the sharp electrode data (cf. Fig. 4). In the whole-cell recordings, the increase in τ_0 with depolarization was seen with negative current steps, with the subsequent positive current step back to the original current, with the relaxation after a short depolarizing current step, and at the end of the current step as the voltage relaxed to RMP (Fig. 7*B*). This increase in τ_0 with depolarization occurred in the linear region of the *I-V* curve, and the total increase in τ_0 was twice as large as the increase in R_N over the tested range of membrane voltage. It was difficult to ascribe the increase in τ_0 solely to an increase in r_m because, for cells whose R_N is dominated by the R_N of electrotonically short processes (see below), both τ_0 and R_N are directly proportional to membrane resistivity (r_m). This can be demonstrated from the definitions of τ_0 and R_N (Jack et al. 1975; Rall 1969, 1977).

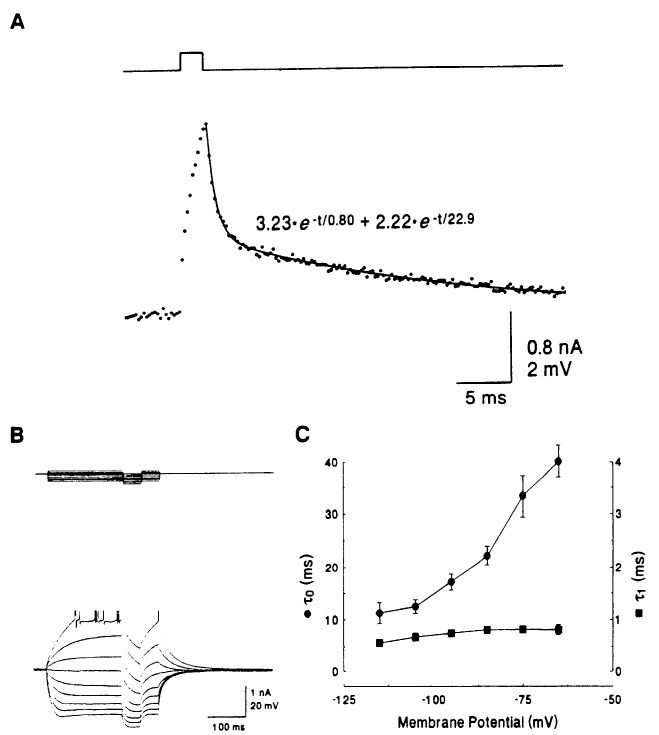

FIG. 7. GC membrane time constants in whole-cell recordings. *A*: protocol used to increase the amplitude of the short exponential term: voltage response to a +200-pA/2-ms current step. *B*: membrane voltage responses (*bottom*) in response to current steps (*top*). Biexponential functions were fit to the initial 50 ms of the charging curve, and also to the voltage response to the 50-ms hyperpolarizing and repolarizing current steps. *C*: τ_1 and τ_0, determined from the 50-ms hyperpolarizing current steps shown in *B*, as a function of the membrane voltage at the start of the hyperpolarizing step. Points are averages of 31 cells; error bars are ±SE. Membrane voltage values are binned in 10-mV increments.

$$\tau_0 = r_m \times c_m$$

$$R_N = 1/G_N = (r_m \times r_i)^{1/2}/\tanh(L) \quad \text{(short cylinder, sealed end)}$$

where c_m is membrane capacitance/unit length; r_m is membrane resistance × unit length; r_i is intracellular resistance/unit length; GN is whole cell conductance. Because

$$L = \text{length} \times (r_m/r_i)^{-1/2} \quad \text{(any cylinder)}$$

Then for $L = 0.5$ (Table 1), $\tanh(L) \approx L$, so that R_N is directly proportional to r_m:

$$R_N = (r_m \times r_i)^{1/2}/[\text{length} \times (r_m/r_i)^{-1/2}] = r_m/\text{length}$$

Although the membrane capacitance is ordinarily not considered to vary with membrane potential, in fact it is determined in part by local polarization due to the voltage-dependent position of membrane-bound charged groups (Fernandez et al. 1982). The voltage dependence of the membrane capacitance has been demonstrated by other investigators (Fernandez et al. 1982; Sutor and Hablitz 1989) and may account for the greater increase in τ_0 relative to R_N at depolarized membrane potentials.

ρ and L for the cells recorded with sharp electrodes were within the range obtained by other investigators with the use of similar recording techniques (Brown et al. 1981; Durand et al. 1983). The data from the whole-cell records led to estimates of ρ and L that were quite different from the sharp electrode values. ρ of 2.1 and 5.1 for the sharp and whole-cell recordings, respectively, indicate that somatic conductances contributed about 1/3 of the total input conductance of the cells recorded with the sharp electrodes, but only 1/6 of the total conductance of the cells recorded with the patch electrodes. ρ is a measure of the departure of the initial charging curve from monoexponential behavior and is strongly affected by the term C_1/τ_1. Some of the difference in ρ between the sharp and whole-cell recordings may reflect an improved high-frequency response in the whole-cell recordings due to the smaller electrode resistance.

In agreement with previous studies (Brown et al. 1981) the correlation between ρ and R_N was low ($r = 0.18$) for whole-cell recordings. This suggests that R_N is determined primarily by factors that affect the soma and cell processes equally in both sharp electrode and whole-cell recordings.

The larger value of L in the sharp electrode vs whole-cell recordings (Table 1) means that the steady-state voltage decay over the physical length of the dendrites is greater in the sharp electrode versus whole-cell recordings. Because the length constant λ is determined by the ratio of the membrane to intracellular resistivity, either an increase in intracellular resistivity or a decrease in r_m would explain the

decrease in λ obtained in sharp electrode recordings. Calculation of the average R_N of the equivalent cylinder representing the cell processes (Table 1) indicates that λ is decreased in sharp electrode recordings because of a decreased r_m relative to the whole-cell recordings.

The values of ρ and L in sharp electrode recordings combine to increase the value of the length constant of the entire GC considered as a finite, sealed-end cylinder (L_C). L is a more appropriate value for estimating the steady-state space clamping of the GC processes, but L_C is a much more easily derived value and is not far from the value of L in whole-cell recordings.

DISCUSSION

Nature of the additional conductance in the sharp electrode recordings

The differences in the RMP, R_N, ρ, and L of the GCs recorded with the sharp versus whole-cell electrodes suggests the presence of an additional transmembrane conductance in the sharp electrode recordings. As demonstrated in the APPENDIX, this conductance is three times larger than the input conductance of the cells recorded with whole-cell techniques and reverses near the RMP. It is possible that chloride ions carry the additional conductance, because the reversal is near the chloride equilibrium potential. However, if the additional conductance were carried by chloride, an overwhelming depolarization would be expected with KCl electrodes; this has not been seen (Fournier and Crepel 1984; Haas and Rose 1987). In addition, the chloride conductance measured in hippocampal pyramidal cells is too small to explain the additional conductance (Thompson and Gähwiler 1990; Thompson et al. 1988). If chloride ions do not carry the additional conductance, then the reversal potential suggests that the additional conductance is due to more than one ionic conductance.

The additional conductance cannot be explained solely by nonspecific leakage of ions across an area of membrane injured by the electrode. First, such a leak conductance would presumably reverse at 0 mV, which is not consistent with the measured values of R_N and RMP in sharp electrode and whole-cell recordings (see Fig. 8 and APPENDIX). Second, the membrane time constant would be more dramatically affected by a leak conductance that was in close proximity to the electrode, because the entire leak conductance would be in parallel with the capacitance of the soma. Third, the difference in the dendritic conductance in the sharp versus whole-cell recordings (Table 1) is not explained by an electrode-associated leak. Although the dendritic conductance in Rall's model actually refers to the conductance of the imperfectly space-clamped portion of the cell, the difference in this conductance in the sharp and whole-cell recordings indicates that the additional conductance in the sharp electrode recordings is not confined to the area immediately surrounding the electrode.

The additional conductance may be due to selection of cells with different R_N by the two techniques. Selection of cells for whole-cell recording is based on increase in electrode resistance as the cell abuts the target membrane; presumably this increase will be more noticeable if the electrode encounters a high-resistance membrane. However, because the data we obtained from sharp electrode and whole-cell recordings are similar to what has been seen in cultured cell preparations (Segal and Barker 1984, 1988), where cell selection is based on other factors, it is unlikely that differential cell selection explains all the differences in the sharp and whole-cell data.

The additional conductance seen in the sharp electrode recordings may be due to a combination of a nonspecific leak conductance due to local electrode-associated membrane injury and a more distributed potassium conduc-

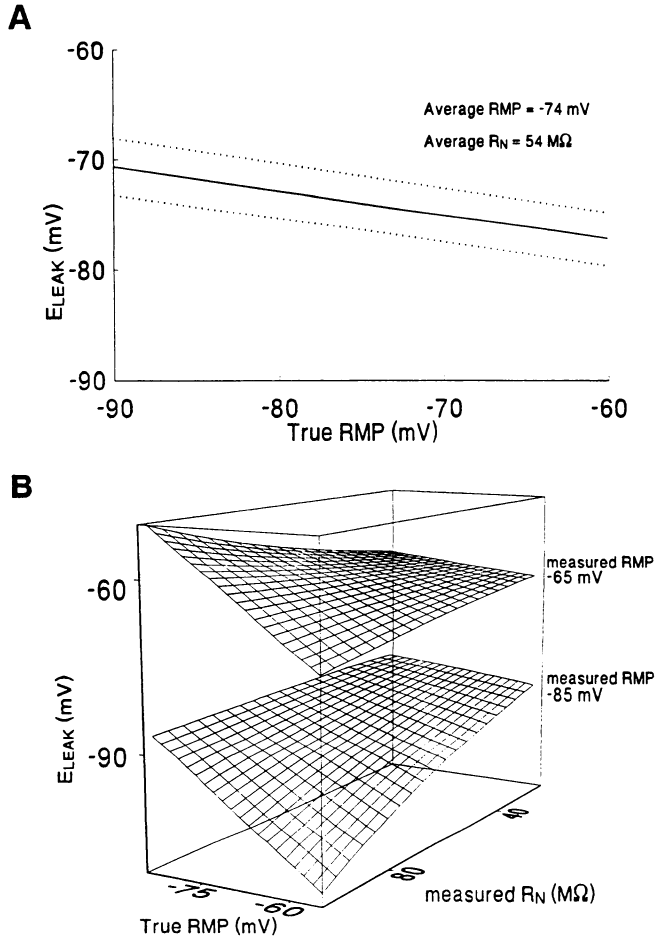

FIG. 8. *A*: possible values of the reversal potential of the additional conductance seen in the sharp electrode recordings ($V_{0Lse} = E_{LEAK}$), given the measured RMPs, the measured G_Ns, and, assuming that for each cell $G_N = G_R + G_L$, and $1/G_R = 228$ MΩ. The true RMP is the potential that would be measured if $G_L = 0$. The solid line is the average relationship of the E_{LEAK} to the true RMP for 11 cells recorded with sharp electrodes (*Eq. 14*); the dotted lines are ±SE. For any reasonable value of the true RMP, E_{LEAK} is near the measured RMP. *B*: Reversal potential of the additional conductance (E_{LEAK}) present in sharp electrode recordings is close to the measured RMP for previously reported values of RMP and R_N. The 2 surfaces represent solutions to *Eq. 14* for 2 different values of measured RMP, when values of measured R_N range from 25 to 100 MΩ, and $1/G_R$ = 228 MΩ. With the use of values of R_N and RMP measured with sharp electrodes in our study or others (Biscoe and Duchen 1985; Crunelli et al. 1983; Haas and Rose 1987; Lambert and Jones 1990; Mody et al. 1988), the relationships of E_{LEAK} to true RMP generated from *Eq. 14* are lines that lie between these two surfaces.

tance that may be modulated by calcium (Lancaster and Adams 1986) and/or sodium (Haiman et al. 1990; Schwindt et al. 1989) entering via the membrane leak. Such a combination of conductances could have a reversal potential near the RMP. The potassium conductance might be supplied by potassium diffusion from the electrode and thus would not require activation of the Na-K adenosine triphosphatase (ATPase); this would explain the relatively small effects of ouabain on the RMP and R_N in hippocampal neurons (McCarren and Alger 1987), despite the magnitude of the additional conductance. Finally, the potassium conductance need not be limited to the area immediately surrounding the electrode; an increase in the conductance of the dendrites would explain the relatively smaller effect of the additional conductance on τ_0 relative to R_N and the decreased dendritic R_N in the sharp electrode recordings. Although the roles of calcium and sodium are speculative, lowered extracellular Ca^{2+} and inorganic Ca^{2+} antagonists have been shown to decrease the RMP and increase the R_N of cells recorded with sharp electrodes (Crunelli et al. 1984; Godfraind 1985; Jones and Heinemann 1987). Similarly, if the difference in spike height in the sharp and whole-cell recordings were due to increased intracellular sodium in the sharp electrode recordings, then a persistent sodium-dependent potassium current (Haiman et al. 1990; Schwindt et al. 1989) might contribute to the difference in R_N. Such a current might explain the increase in R_N seen in sharp electrode recordings with lowered extracellular sodium (Segal and Barker 1984).

Electrotonic parameters

Dentate gyrus GCs recorded with the whole-cell technique have substantially increased R_Ns and are more compact electrotonically than sharp electrode recordings have indicated. These findings are consistent with the results from other preparations (Coleman and Miller 1989). The analysis is based on a model that makes a number of simplifying assumptions about the nature of the GC structure (Rall 1977); not all of these assumptions may be accurate in the case of dentate GCs. Because the model assumes a uniform dendritic r_m, the spontaneous synaptic activity that was present in our slices (Otis et al. 1991; Staley and Mody 1991; Staley et al. 1990) would affect the accuracy of our results unless the physical distribution, frequency, amplitude, and type of synaptic activity were uniform; there is no way to determine how closely this condition was met. The change in electrotonic parameters with more intense synaptic activity provides the basis for shunting inhibition (Staley and Mody 1992). GC processes that are of unequal length or that do not branch in a way to preserve the (diameter)$^{3/2}$ relation between the trunk and the branches will decrease the accuracy of the equivalent cylinder representation; there is some evidence that this is the case (Desmond and Levy 1984). Finally, the cell soma in the electrotonic sense is that portion of the cell which is perfectly space clamped; the physical extent of this portion of the cell is unknown. Given the small value of L, this uncertainty is not very significant, but it complicates comparisons of the electrotonic parameters of sharp and whole-cell recordings.

The whole-cell recordings indicate that the GCs have a high dendritic-to-somatic conductance and a short dendritic electrotonic length; this is a unique electrotonic structure that has not been previously reported. The short electrotonic distance of the dendrites indicates that, despite the physically extended structure of the GC processes, the decrement in DC membrane voltage is small over the length of the process.

The extent of the steady-state voltage decrement along the length of a cell process can be estimated by considering the ratio of voltage at the proximal end of the process (which is equal to the electrode voltage, because the soma is considered a lumped circuit) to the voltage at a distance equal to L, the most distant point on the equivalent cylinder. With the use of the expression derived by Rall (1969) and Jack et al. (1975)

$$V/V_0 = 1/\cosh(L)$$

For the whole-cell recordings, the average value of V/V_0 is 0.90. For the sharp electrode recordings, V/V_0 is 0.79. Thus the DC voltage error due to imperfect space clamp in the GC processes is only 10% for whole-cell recordings; this is a substantial improvement over the 33–40% decrement suggested by earlier studies (Brown et al. 1981a; Durand et al. 1983).

Voltage decrements along the dendrites may be much larger for voltage transients, which are filtered by the dendritic membrane capacitance (Carnevale and Johnston 1982; Rall 1977; Rall and Segev 1985). In fact, the long τ_0 of the GCs indicates that short currents from synaptic activity will be substantially filtered (cf. Fig. 7). However, a critical feature of the electrotonic structure of the GCs revealed by whole-cell recordings is that the information in these transients is not lost via shunting across a low membrane resistance. Rather, the information is spread out over time by the charging and discharging of the membrane capacitance. This decreases the effect of any one synaptic event but increases the time period over which the effects of two distinct synaptic events will be additive at the cell soma.

APPENDIX

Input conductances in sharp and whole-cell recordings

ASSUMPTION 1. In analogy to the derivation of Hodgkin and Horowicz (1959) for ionic conductances, the measured GC input conductance (G_N) can be represented as a linear combination of the true resting conductance (G_R) and an additional conductance (G_L) which is induced by the electrode

$$G_N = 1/R_N = G_R + G_L \qquad (1)$$

ASSUMPTION 2. The difference in R_N between the sharp and whole-cell recordings is due to a difference in G_L. This does not automatically follow from assumption 1, because the sharp and whole-cell recording techniques may select for cells with different G_R.

On the basis of the relative values of R_N, the additional conductance associated with the whole-cell electrodes must be negligible compared to the additional conductance associated with the sharp

electrodes; we therefore approximate G_R as the G_N of the whole-cell records

$$G_R \approx G_{Nwc} \quad (2)$$

$$G_{Nse} \approx G_{Nwc} + G_{Lse} \quad (3)$$

Where the subscript se refers to sharp electrode recordings and the subscript wc refers to whole-cell recordings. Then the current-voltage relationship in the linear region around the RMP can be described for whole-cell recordings as

$$I_{wc} = G_{Nwc} \times (V - V_{0wc}) \quad (4)$$

or rewritten as

$$V = (1/G_{Nwc}) \times I + V_{0wc} \quad (5)$$

where

$$V_{0wc} = \mathrm{RMP}_{wc}$$

for the sharp electrode data with the approximation of *Eq. 2*

$$I = G_{Nwc} \times (V - V_{0se}) + G_{Lse} \times (V - V_{0Lse}) \quad (6)$$

or rewritten as

$$V = (G_{Nwc} + G_{Lse})^{-1} \times I + (G_{Nwc} \times V_{0se} + GLse \times V_{0Lse})/(G_{Nwc} + G_{Lse}) \quad (7)$$

Where V_{0se} is RMP_{se} (the true RMP of the cell if there were no leak conductances) and V_{0Lse} is reversal potential of the sharp electrode-associated additional conductance. The slope of the line in equation 5 is $1/G_{Nwc}$; the slope of *Eq. 7* is $1/(G_{Nwc} + G_{Lse})$; with the use of appropriate values for R_N for sharp electrode and whole-cell recordings (cf. Fig. 5), we obtain

$$1/G_{Lse} = 71\,M\Omega \quad (8)$$

The slow inward rectifier conductance in sharp and whole-cell recordings

We can extend assumptions 1 and 2 to describe the conductance (G_{NH}) in the region in which the slow inward rectifier conductance (G_Q) is fully activated

$$G_{NH} = G_R + G_L + G_Q \quad (9)$$

With the use of the approximation of *Eq. 2*, the conductance for the whole-cell and sharp electrode data is written

$$G_{NHwc} \approx G_{Nwc} + G_{Qwc} \quad (10)$$

$$G_{NHse} \approx G_{Nwc} + G_{Lse} + G_{Qse} \quad (11)$$

Then, as in *Eq. 4–7*, the voltage can be written as a function of current

$$V_{Hwc} = (G_{Nwc} + G_{Qwc})^{-1\times1} + (G_{Nwc} \times \mathrm{RMP}_{wc} + G_{Qwc} \times V_{0Qwc})/(G_{Nwc} + G_{Qwc}) \quad (12)$$

$$V_{Hse} = (G_{Nwc} + G_{Lse} + G_{Qse})^{-1\times1} + (G_{Nwc} \times V_{0Rse} + G_{Lse} \times V_{0Lse} + G_{Qse} \times V_{0Qse})/(G_{Nwc} + G_{Lse} + G_{Qwc}) \quad (13)$$

The slopes of the lines described by *Eq. 12* and *13* are $(G_{Nwc} + G_{Qwc})^{-1}$ and $(G_{Nwc} + G_{Lse} + G_{Qse})^{-1}$, respectively. With the use of the appropriate slope conductances (cf. Fig. 5), and the previously derived value for G_{Lse}

$$1/G_{Qwc} = 202\,M\Omega$$

$$1/G_{Qse} = 118\,M\Omega$$

Reversal potential of the additional conductance

When $I = 0$, *Eq. 13* reduces to the Hodgkin-Horowicz equation (Hodgkin and Horowicz 1959). Rewriting *Eq. 7* with $I = 0$, and substituting $1/R_{Nse}$ for $(G_{Nwc} + G_{Lse})$,

$$V_{0Lse} = (-G_{Nwc}/G_{Lse}) * V_{0se} + \mathrm{RMP}_{se}/(R_{Nse} \times G_{Lse}) \quad (14)$$

This gives the linear relation of the reversal potential of the additional electrode-associated conductance, V_{0Lse}, to the true RMP of the cells recorded with sharp electrodes, V_{0se}. The measured resting potential of the whole-cell records cannot be accurately substituted for the true resting potential of the sharp electrode recordings because the recording conditions were somewhat different. The relation of the reversal potential of the electrode-associated conductance to the true RMP of the sharp electrode recordings is plotted in Fig. 8. Figure 8 indicates that the measured RMP equals the true RMP only when the electrode-associated conductance reverses at the true RMP. Figure 8*B* demonstrates that the reversal potential of the additional leak conductance must be near the measured RMP for any reasonable values of the true RMP (V_{0se}) and measured R_N.

We would like to thank J. T. Palmer and I. Parada for technical assistance, John Dempster for providing the Strathclyde Electrophysiology software, and John Huguenard for helpful discussions.

This research was supported by a Dana Postdoctoral Fellowship to K. J. Staley, a Howard Hughes Predoctoral Fellowship to T. S. Otis, a Klingenstein Fellowship and National Institute of Neurological Disorders and Stroke Grants NS-12151 and NS-27528 to I. Mody.

Address for reprint requests: K. J. Staley, Dept. of Neurology, B182, Univ. of Colorado, Denver, CO 80262.

Received 1 April 1991; accepted in final form 13 January 1992.

REFERENCES

ADAMS, P. R. AND HALLIWELL, J. V. A hyperpolarization-induced current in hippocampal pyramidal cells. *J. Physiol. Lond.* 324: 62–63, 1982.

BEN-ARI, Y., CHERUBINI, E., CORRADETTI, R., AND GAIARSA, J. L. Giant synaptic potentials in immature rat CA3 hippocampal neurones. *J. Physiol. Lond.* 416: 303–325, 1989.

BISCOE, T. J. AND DUCHEN, M. R. An intracellular study of dentate, CA1, and CA3 neurons in the mouse hippocampal slice. *Q. J. Exp. Physiol.* 70: 189–202, 1980.

BLANTON, M. G., LO TURCO, J. L., AND KRIEGSTEIN, A. R. Whole-cell recording from neurons in slices of reptilian and mammalian cortex. *J. Neurosci. Methods* 30: 203–210, 1989.

BROWN, D. A., GÄHWILER, B. H., GRIFFITH, W. H., AND HALLIWELL, J. V. Membrane currents in hippocampal neurons. *Prog. Brain Res.* 83: 141–160, 1990.

BROWN, K. M. AND DENNIS, J. S. Derivative free analogs of the Levenberg-Marquardt and Gauss algorithms for non-linear least squares approximation. *Num. Mathemat.* 18: 289–297, 1972.

BROWN, T. H., FRICKE, R. A., AND PERKEL, D. H. Passive electrical constants in three classes of hippocampal neurons. *J. Neurophysiol.* 46: 812–827, 1981a.

BROWN, T. H., PERKEL, D. H., NORRIS, J. C., AND PEACOCK, J. H. Electrotonic structure and specific membrane properties of mouse dorsal root ganglion cells. *J. Neurophysiol.* 45: 1–15, 1981b.

CARNEVALE, N. T. AND JOHNSTON, D. Electrophysiological characterization of remote chemical synapses. *J. Neurophysiol.* 47: 606–621, 1982.

COLE, K. S. AND MOORE, J. W. Liquid junction and membrane potentials of the squid giant axon. *J. Gen. Physiol.* 43: 971–980, 1959.

COLEMAN, P. A. AND MILLER, R. F. Measurement of passive membrane parameters with whole-cell recording from neurons in the intact amphibian retina. *J. Neurophysiol.* 61: 218–230, 1989.

CRUNELLI, V., FORDA, S., AND KELLY, J. S. Blockade of amino acid-induced depolarizations and inhibition of excitatory post-synaptic potentials in rat dentate gyrus. *J. Physiol. Lond.* 341: 627–640, 1983.

CRUNELLI, V., FORDA, S., AND KELLY, J. S. The reversal potential of excitatory amino acid action on granule cells of the rat dentate gyrus. *J. Physiol. Lond.* 351: 327–342, 1984.

DESMOND, N. L. AND LEVY, W. B. Dendritic caliber and the $^3/_2$ power relationship of dentate granule cells. *J. Comp. Neurol.* 227: 589–596, 1984.

DURAND, D., CARLEN, P. L., GUREVICH, N., HO, A., AND KUNOV, H. Electrotonic parameters of rat dentate granule cells measured using short current pulses and HRP staining. *J. Neurophysiol.* 50: 1080–1097, 1983.

EDWARDS, F. A., KONNERTH, A., SAKMANN, B., AND TAKAHASHI, T. A thin slice preparation for patch clamp recordings from neurones of the mammalian central nervous system. *Pfluegers Arch.* 414: 600–612, 1989.

FERNANDEZ, J. M., BEZANILLA, F., AND TAYLOR, R. E. Distribution and kinetics of membrane dielectric polarization. II. Frequency domain studies of gating currents. *J. Gen. Physiol.* 79: 41–67, 1982.

FINKEL, A. S. AND REDMAN, S. J. Optimal voltage clamping with a single microelectrode. In: *Voltage and Patch Clamping with Microelectrodes,* edited by T. G. Smith, H. Lecar, S. J. Redman, and P. W. Gage. Bethesda, MD: Am. Physiol. Soc. 1985, p. 95–120.

FOURNIER, E. AND CREPEL, F. Electrophysiological properties of dentate granule cells in mouse hippocampal slices maintained in vitro. *Brain Res.* 311: 75–86, 1984.

FRICKE, R. A. AND PRINCE, D. A. Electrophysiological properties of dentate granule cells. *J. Neurophysiol.* 51: 195–209, 1984.

GAGNE, S. AND PLAMONDON, R. Tip potential of open-tip microelectrodes: theoretical and experimental studies. *Can. J. Physiol. Pharmacol.* 61: 857–869, 1982.

GODFRAIND, G. M. Intrasomatic and intradendritic recordings of plateau potentials in slices of the dentate gyrus maintained in vitro. *Exp. Brain Res.* 57: 233–238, 1985.

GRYNKIEWICZ, G., POENIE, M., AND TSIEN, R. Y. A new generation of Ca^{2+} indicators with greatly improved fluorescence properties. *J. Biol. Chem.* 260: 3440–3450, 1985.

HAAS, H. L. AND ROSE, G. M. Noradrenaline blocks potassium conductance in rat dentate gyrus granule cells in vitro. *Neurosci. Lett.* 78: 171–174, 1987.

HAGIWARA, S. AND OHMORI, H. Studies of calcium channels in rat clonal pituitary cells with patch electrode voltage-clamp. *J. Physiol. Lond.* 331: 231–252, 1982.

HAIMAN, C., BERNHEIM, L., BERTRAND, D., AND BADER, C. R. Potassium current activated by intracellular sodium in quail trigeminal ganglion cells. *J. Gen. Physiol.* 95: 961–979, 1990.

HAKOZAKI, S., MATSUMOTO, M., AND SASAKI, K. Temperature-sensitive activation of G-protein regulating the resting membrane conductance of *Aplysia* neurons. *Jpn. J. Physiol.* 39: 115–130, 1989.

HAMILL, O. P., MARTY, A., SAKMANN, B., AND SIGWORTH, F. J. Improved patch-clamp technique for high-resolution current recording from cells and cell-free membrane patches. *Pfluegers Arch.* 391: 85–100, 1981.

HARRISON, S. M. AND BERS, D. M. The effect of temperature and ionic strength on the apparent Ca-affinity of EGTA and the analogous Ca-chelators BAPTA and dibromo-BAPTA. *Biochim. Biophys. Acta* 925: 133–143, 1987.

HESTRIN, S., NICOLL, R., PERKEL, D., AND SAH, P. Analysis of excitatory synaptic action in the rat hippocampus using whole-cell recording from thin slices. *J. Physiol. Lond.* 422: 203–225, 1990.

HODGKIN, A. L. AND HOROWICZ, P. The influence of potassium and chloride ions on the membrane potential of single muscle fibres. *J. Physiol. Lond.* 148: 127–160, 1959.

HORIKAWA, K. AND ARMSTRONG, W. E. A versatile means of intracellular labeling: injection of biocytin and its detection with avidin conjugates. *J. Neurosci. Methods* 25: 1–11, 1988.

HORN, R. AND MARTY, A. Muscarinic activation of ionic currents measured by a new whole-cell recording method. *J. Gen. Physiol.* 92: 145–159, 1988.

HOTSTON, J. R., PRINCE, D. A., AND SCHWARTZKROIN, P. A. Anomalous rectification in hippocampal neurons. *J. Neurophysiol.* 42: 889–895, 1979.

JACK, J. J. B., NOBLE, D., AND TSIEN, R. W. *Electric Current Flow in Excitable Cells.* London: Oxford Univ. Press, 1975.

JOHNSTON, D. Passive cable properties of hippocampal CA3 pyramidal neurons. *Cell Mol. Neurobiol.* 1: 41–55, 1981.

JOHNSTON, D. AND BROWN, T. H. Interpretation of voltage-clamp measurements in hippocampal neurons. *J. Neurophysiol.* 50: 464–486, 1983.

JONES, R. S. G. AND HEINEMANN, U. Abolition of the orthodromically evoked IPSP of CA1 cells before the EPSP during washout of calcium from hippocampal slices. *Exp. Brain Res.* 65: 676–680, 1987.

KAWAGUCHI, Y. AND HAMA, K. Two subtypes of non-pyramidal cells in rat hippocampal formation identified by intracellular recordings and HRP injection. *Brain Res.* 411: 190–195, 1987.

KÖHR, G. AND MODY, I. Endogenous intracellular calcium buffering and the activation/inactivation of HVA calcium currents in rat dentate gyrus granule cells. *J. Gen. Physiol.* 98: 941–967, 1991.

KRIEGSTEIN, A. R., SUPPES, T., AND PRINCE, D. A. Cellular and synaptic physiology and epileptogenesis of developing rat neocortical neurons in vitro. *Dev. Brain Res.* 34: 161–171, 1987.

LAMBERT, J. D. C. AND JONES, R. S. G. A reevaluation of excitatory amino-acid mediated synaptic transmission in the rat dentate gyrus. *J. Neurophysiol.* 64: 119–132, 1990.

LANCASTER, B. AND ADAMS, P. R. Calcium-dependent current generating the afterhyperpolarization of hippocampal neurons. *J. Neurophysiol.* 55: 1268–1282, 1986.

LANCASTER, B. AND NICOLL, R. A. Properties of two calcium-activated hyperpolarizations in rat hippocampal neurons. *J. Physiol. Lond.* 389: 187–203, 1987.

LLANO, I., LERESCHE, N., AND MARTY, A. Calcium entry increases the sensitivity of cerebellar Purkinje cells to applied GABA and decreases inhibitory synaptic currents. *Neuron* 6: 565–574, 1991.

MADISON, D. V. AND NICOLL, R. A. Control of the repetitive discharge of rat CA1 pyramidal neurones in vitro. *J. Physiol. Lond.* 354: 319–331, 1984.

MALINOW, R. AND TSIEN, R. Presynaptic enhancement shown by whole-cell recordings of long-term potentiation in hippocampal slices. *Nature Lond.* 346: 177–180, 1990.

MCCARREN, M. AND ALGER, B. E. Sodium-potassium pump inhibitors increase neuronal excitability in the rat hippocampal slice: role of a Ca^{2+}-dependent conductance. *J. Neurophysiol.* 57: 496–509, 1987.

MCCORMICK, D. A. AND PAPE, H.-C. Properties of a hyperpolarization-activated current and its role in rhythmic oscillation in thalamic relay neurones. *J. Physiol. Lond.* 431: 291–318, 1990.

MCNAUGHTON, B. L., BARNES, C. A., AND ANDERSEN, P. Synaptic efficacy and EPSP summation in granule cells of rat fascia dentata studied in vitro. *J. Neurophysiol.* 46: 952–966, 1981.

MODY, I. AND OTIS, T. S. Whole-cell patch-clamp recordings in adult rat hippocampal slices. *Soc. Neurosci. Abstr.* 15: 1309, 1989.

MODY, I., STANTON, P. K., AND HEINEMANN, U. Activation of *N*-methyl-D-aspartate receptors parallels changes in cellular and synaptic properties of dentate gyrus genule cells after kindling. *J. Neurophysiol.* 59: 1033–1054, 1988.

OTIS, T. S., STALEY, K. J., AND MODY, I. Perpetual inhibitory activity in mammalian brain slices generated by spontaneous GABA release. *Brain Res.* 545: 142–150, 1991.

PETHIG, R., KUHN, M., PAYNE, R., ADLER, E., CHEN, T.-H., AND JAFFE, L. F. On the dissociation constant of BAPTA-type calcium buffers. *Cell Calcium* 10: 491–498, 1989.

PUSCH, M. AND NEHER, E. Rates of diffusional exchange between small cells and a measuring patch pipette. *Pfluegers Arch.* 411: 204–211, 1988.

RALL, W. Time constants and electrotonic length of membrane cylinders and neurons. *Biophys. J.* 9: 1483–1508, 1969.

RALL, W. Core conductor theory and cable properties of neurons. In: *Handbook of Physiology. The Nervous System. Cellular Biology of Neurons.* Bethesda, MD: Am. Physiol. Soc., 1977, sect. 1, vol. I, part 1, p. 39–97.

RALL, W. AND SEGEV, I. Space clamp problems when voltage clamping branched neurons with intracellular microelectrodes. In: *Voltage and Patch Clamping with Microelectrodes,* edited by T. G. Smith, H. Lecar, S. J. Redman, and P. W. Gage. Baltimore, MD: Am. Physiol. Soc. 1985, p. 191–215.

SCHWINDT, P. C., SPAIN, W. J., AND CRILL, W. E. Long-lasting reduction

of excitability by a sodium-dependent potassium current in cat neocortical neurons. *J. Neurophysiol.* 61: 233–244, 1989.

SEGAL, M. AND BARKER, J. L. Rat hippocampal neurons in culture: potassium conductances. *J. Neurophysiol.* 51: 1409–1433, 1984.

SEGAL, M. AND BARKER, J. L. Outward rectification of inhibitory postsynaptic currents in cultured rat hippocampal neurones. *J. Physiol. Lond.* 403: 41–55, 1988.

SERESS, L. AND POKORNY, J. Structure of the granular layer of the rat dentate gyrus. A light microscopic and Golgi study. *J. Anat.* 133: 181–195, 1981.

SHEN, K. AND SCHWARTZKROIN, P. A. Effects of temperature alterations on population and cellular activities in hippocampal slices from mature and immature rabbit. *Brain Res.* 475: 305–316, 1988.

SNEDECOR, G. W. AND COCHRAN, W. G. *Statistical Methods.* Ames, IA: Iowa Univ. Press, 1975.

STALEY, K. J. AND MODY, I. Integrity of perforant path fibers and the frequency of action potential independent spontaneous excitatory and inhibitory synaptic events in dentate gyrus granule cells. *Synapse* 9: 219–224, 1991.

STALEY, K. J. AND MODY, I. Shunting of excitatory input to dentate gyrus granule cells by a depolarizing $GABA_A$ receptor-mediated conductance. *J. Neurophysiol.* In press.

STALEY, K. J., OTIS, T., AND MODY, I. Action potential insensitive spontaneous excitatory synaptic transmission in dentate gyrus granule cells. *Soc. Neurosci. Abstr.* 16: 167, 1990.

STORM, J. F. Why is the input conductance of hippocampal neurons impaled with microelectrodes so much higher than when giga-seal patch pipettes are used? *Soc. Neurosci. Abstr.* 16: 506, 1990a.

STORM, J. F. Potassium currents in hippocampal pyramidal cells. *Prog. Brain Res.* 83: 161–187, 1990b.

SUTOR, B. AND HABLITZ, J. J. EPSPs in rat neocortical neurons in vitro I. Electrophysiological evidence for two distinct EPSPs. *J. Neurophysiol.* 61: 607–620, 1989.

THOMPSON, S. M., DEISZ, R. A., AND PRINCE, D. A. Relative contributions of passive equilibrium and active transport to the distribution of chloride in mammalian cortical neurons. *J. Neurophysiol.* 60: 105–124, 1988.

THOMPSON, S. M. AND GÄHWILER, B. H. Activity-dependent disinhibition. II. Effects of extracellular potassium, furosemide, and membrane potential on E_{Cl^-} in hippocampal CA3 neurons. *J. Neurophysiol.* 61: 512–523, 1990.

VANYSEK, P. Activity coefficients of acids, bases and salts. In: *Handbook of Chemistry and Physics,* edited by R. C. Weast. Boca Raton, FL: CRC, 1988, p. D-169.

WILSON, C. J. AND PARK, M. R. Capacitance compensation and bridge balance adjustment in intracellular recording from dendritic neurons. *J. Neurosci. Methods* 27: 51–75, 1989.